Technical University of Denmark

DTU

Bistability and low-frequency fluctuations in semiconductor lasers with optical feedback: a theoretical analysis

Mørk, Jesper; Tromborg, Bjarne; Christiansen, Peter Leth

DTU Library
Technical Information Center of Denmark

Regular Papers

Bistability and Low-Frequency Fluctuations in Semiconductor Lasers with Optical Feedback: A Theoretical Analysis

JESPER MØRK, BJARNE TROMBORG, AND PETER L. CHRISTIANSEN

Abstract—Near-threshold operation of a semiconductor laser exposed to moderate optical feedback may lead to low-frequency fluctuations. In the same region, a kink is observed in the light–current characteristic. We demonstrate that these nonlinear phenomena are predicted by a noise-driven multimode traveling wave model. The dynamics of the low-frequency fluctuations are explained qualitatively in terms of bistability through an iterative description.

I. INTRODUCTION

OPTICAL feedback from an external cavity can have a profound impact on the dynamics and spectral behavior of semiconductor lasers [1]-[17]. At low levels of optical feedback, a significant linewidth reduction and improved frequency stability are obtained [2]-[5], which is important for such applications as coherent transmission systems and interferometric fiber sensors. For a laser diode coupled to a single-mode fiber the Rayleigh backscatter-induced line narrowing can result in linewidths in the subhertz region [6]. Higher feedback levels may, however, result in laser line broadening to a width of several GHz [4], [7]-[10]. Also, a kink in the light–current characteristic is observed near the threshold of the solitary laser [10]-[13]. In the same region, the time evolution of the light intensity shows a characteristic pattern of low-frequency fluctuations (LFF). The experimentally observed pattern [10], [12]-[15] has qualitatively the appearance of the trace in Fig. 1 (obtained by computer simulation). From a level (approximately) given by the feedback the intensity shows a randomly occurring sudden drop to a low value followed by a stepwise buildup to the original level. The steplength is equal to the round-trip time τ in the external cavity, and the buildup requires about 10 steps. In this paper we present a theoretical investigation of these phenomena related to higher feedback levels (greater than -30 dB). The paper may be considered as an extension of the works of Ries and Sporleder [13], [16] and Henry and Kazarinov [17] with emphasis

on the dynamics of the LFF and its relation to the kinked light–current characteristics.

The theoretical investigations of the external cavity configuration are commonly based on the model of Lang and Kobayashi [1], which is obtained by adding a time-delayed term to the usual rate equation for the complex field, thus yielding a nonlinear delay-differential equation. The rich variety of phenomena encountered experimentally when operating a semiconductor laser in an external cavity may be appreciated by the very complex dynamics of such equations, see, e.g., [18].

The linewidth reduction and stability properties at low feedback levels are generally obtained from a linear small-signal version of the rate equations, see, e.g., [6], [9], [19], and [20]. At higher feedback levels one observes a saturation of linewidth reduction followed by an abrupt transition to a state characterized by a very broad laser line [4], [8], [9]. By computer simulations this behavior was also found to be contained in the model of Lang and Kobayashi and to be a consequence of the nonlinear dynamics [9]. The first detailed experimental and theoretical investigation of the state of increased linewidth was performed by Lenstra *et al.* [8]. They introduced the concept of "coherence collapse" to describe the dramatic transition from a state of long coherence length to the line broadened state of short coherence length. As pointed out in [8] and [9], the increased linewidth may be a result of chaotic dynamics, which has also been suggested for the external cavity configuration in [21]-[24]. A survey of chaos in semiconductor laser devices and additional references are given in [25]. In [17] the appearance of LFF is explained as a result of a second-order instability in the rate equations with constant feedback, and the increased linewidth is seen merely as a result of the frequency chirp associated with these fluctuations. The route to chaos studied by Mukai and Otsuka [22], [23], goes through a passive mode-locking type of oscillations at harmonics or subharmonics of the external cavity roundtrip frequency. These phenomena occur when the roundtrip frequency is close to the relaxation oscillation frequency, and here the anomalous interaction described by Bogatov *et al.* [26] is shown to play a dominant role. The LFF will be shown to have a different origin.
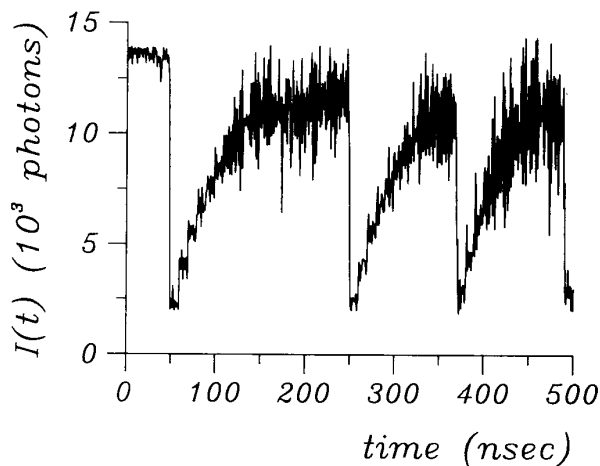
Generally, in dealing theoretically with strongly non-

Fig. 1. Simulated time evolution of total photon number $I(t)$. Laser biased at solitary threshold $J = J_{th}$, power feedback ratio $\kappa^2 = 0.0225$ (-16.5 dB), $\tau = 10$ ns.

linear states of the external cavity configuration, one has to employ some kind of reduction of the infinite dimensionality [18] of the governing delay-differential equation in order to obtain at least a qualitative physical understanding of the operating state.

In [8] the coherence collapsed state is described approximately by replacing the delay terms with external noise terms, which are dominant in comparison with the internal spontaneous emission noise. This results in a self-consistent statistical description of the collapsed state, which is in rough agreement with experiments when the autocorrelation function for the electric field shows a single narrow peak. According to this model the coherence collapse gives rise to a change in mean frequency and linewidth, which is also in rough agreement with the results of computer simulations [9].

In [17] the feedback term is replaced by the stationary solution, thus corresponding to an injection locking treatment [27], [28] which is valid in a time interval of the order of the external cavity roundtrip time τ. This allows a rather simple investigation of the stability properties of the stationary state, but any dynamics involving time scales larger than τ is necessarily left out.

In this paper we will show that the LFF may be simulated by a simple traveling wave model [16], [29] and that the dynamics of the LFF may be understood qualitatively from a simple iterative model. Fig. 1 shows an example of a computer simulation of the LFF. A similar result was obtained in [13], [16]. In the iterative model the field power spectra and the carrier densities at different steps of length τ form the essential variables. Owing to the delay in the external cavity the spectrum at one specific step determines the spectrum and the carrier density at the following step. By this approximative approach the LFF are understood as a result of bistability and dynamic formation of bistability.

In Section II we employ the injection locking approximation of [17] and show that the resulting (noise-free) equation may admit another new stationary and stable so-

lution or a limit cycle solution. This bistability makes possible the first power drop in Fig. 1, while the instability found in [17] may be seen as the cause of the transition. The bistability is examined as a function of bias current and found to be absent below a critical pumping level, whereas the nature of the "new" solution changes qualitatively slightly above the threshold of the solitary laser.

In Section III an iterative description of the intensity buildup from the low-power level of Fig. 1 is developed. The inclusion of a Langevin noise term in the field equation is shown to result in a qualitative change in the bistability condition. During the initial buildup of intensity, bistability is absent but is recovered after typically 10 external roundtrip periods, after which a noise-induced switching becomes possible. Bistability occurs before the stationary solution with feedback is reached, and this state need not be recovered. This is in agreement with Fig. 1, where the simulation was initialized with the stationary feedback solution.

In Section IV we present results of direct simulations of a traveling wave model which includes Langevin noise terms accounting for the randomly occurring spontaneous emission events [16], [29]. The model consists of a set of difference equations. The inclusion of several longitudinal modes is found necessary in order to simulate the LFF properly. This is in accordance with the wide multimode spectra observed experimentally [10], [13]. Simulations generally support the approximative "ensemble-averaged" description of Section III but also demonstrate its limitations. The intensity shows large fluctuations around the mean value. However, increasing the rate of spontaneous emission and the number of longitudinal modes has a significant stabilizing effect on the simulated LFF. If the Langevin noise terms are switched off after the first transition the intensity noise persists and even increases. This indicates strongly that we have a case of deterministic chaos. Variation of the bias current around the solitary threshold and calculation of the associated mean intensities demonstrate the kink in the light–current characteristics to be contained in the simulation model. The kink is due to a fast decrease of the LFF period with increasing bias current, which well-above threshold results in seemingly random intensity fluctuations between the stationary solutions with and without feedback. From the simulations we get rough estimates of the lifetime of a coherent state. These estimates turn out to disagree with the predictions of [17].

Finally, Section V summarizes our conclusions.

II. STATIONARY SOLUTIONS AND BISTABILITY

A. Single-Mode Rate Equations

The complex field equation of Lang and Kobayashi [1] may be written (see also [20])

$$\frac{d}{dt} E(t) = \frac{1}{2} (1 + j\alpha) \, G_N (N - N_{th}) \, E(t)$$

$$+ \frac{\kappa}{\tau_{in}} \exp(-j\omega_o \tau) \, E(t - \tau). \qquad (1)$$

Here, $E(t)$ is the slowly varying complex envelope function with $E(t) e^{j\omega_o t} = |E(t)| \exp[j(\omega_o t + \phi(t))]$ being the outgoing field at the internal laser mirror facing the external cavity. The solitary laser is assumed to oscillate in a single longitudinal mode with angular frequency ω_o. The gain per unit time is

$$G(N) = G_N(N - N_o) \tag{2}$$

where N is the carrier density averaged over the active region, and G_N and N_o are constants. The threshold carrier density for the solitary laser N_{th} is related to the photon lifetime τ_p by

$$G(N_{th}) = \frac{1}{\tau_p}. \tag{3}$$

τ_{in} and τ are the roundtrip times in the laser cavity and the external cavity respectively, and κ^2 is the power reflected from the external cavity relative to the power reflected from the laser mirror. Finally, α is the linewidth enhancement factor accounting for the amplitude-phase coupling [30].

The evolution of the carrier density is governed by the usual rate equation

$$\frac{d}{dt} N(t) = J - \frac{N(t)}{\tau_s} - G(N)|E(t)|^2 \tag{4}$$

where J is the constant pumping term and τ_s is the carrier lifetime. We assume $E(t)$ to be normalized such that the total number of photons in the lasing mode is

$$I(t) = V|E(t)|^2 \tag{5}$$

where V is the active region volume.

Equations (1) and (4) neglect the effects of lateral carrier diffusion and spatial hole burning and do not include multiple reflections, i.e., $\kappa^2 \ll 1$. Furthermore, spontaneous emission noise has not been included but will be taken into account in the following sections.

Stationary solutions of (1) and (4) are found by substitution of

$$E(t) = E_s \exp(j\Delta\omega_s t), \qquad N(t) = N_s \tag{6}$$

where E_s, $\Delta\omega_s = \omega_s - \omega_o$, and N_s are real constants. This yields the equations [20]

$$\omega_o\tau = \omega_s\tau + \kappa \frac{\tau}{\tau_{in}} \sqrt{1 + \alpha^2} \sin(\omega_s\tau + \text{Arctan}(\alpha)) \tag{7a}$$

$$N_s = N_{th} - \frac{2\kappa}{G_N\tau_{in}} \cos(\omega_s\tau) \tag{7b}$$

$$E_s^2 = \frac{1}{G(N_s)}\left(J - \frac{N_s}{\tau_s}\right). \tag{7c}$$

The solutions ω_s to (7a) for fixed ω_o are the angular frequencies of the external cavity modes. For $\kappa\tau\sqrt{1 + \alpha^2}/\tau_{in} > 1$, (7a) yields multiple solutions for ω_s [31], and the dominant external cavity mode is identified

as the mode with minimum carrier density N_s. We shall assume that the feedback ratio and external cavity length are large enough $(\alpha\kappa\tau/(2\pi\tau_{in}) \gg 1$, see [17]) that the dominant mode may be taken to satisfy $\omega_s\tau = 0$ (mod 2π), which according to (7b)–(7c) corresponds to maximum output power. Defining a detuning parameter by, [9], $d = \omega_o\tau - \alpha\kappa\tau/\tau_{in}$ (mod 2π), $\omega_s\tau = 0$ (mod 2π) corresponds to $d = 0$, which is ensured experimentally by varying the cavity length within a wavelength or by varying ω_o via bias current or temperature. According to (7b) the threshold current is then reduced from the solitary value $J_{th} = N_{th}/\tau_s$ to the effective value $J'_{th} = J_{th} - 2\kappa/(G_N\tau_{in}\tau_s)$. In the following, we use the set of parameters specified in Table I.

B. Injection of Stationary Feedback Field

Starting from a stationary state with feedback, the delay term in (1) may be replaced by injection of the stationary solution (7) while keeping the field inside the laser as a variable. This yields the equation

$$\frac{d}{dt} E(t) = \frac{1}{2}(1 + j\alpha) G_N(N - N_{th}) E(t)$$
$$+ \frac{\kappa}{\tau_{in}} E_s \exp(j\Delta\omega_s t) \tag{8}$$

which holds in a time interval of length τ.

Assuming a quasi-stationary solution which is locked to the injected field we have

$$E(t) = E_l \exp[j(\Delta\omega_s t + \phi_l)] \tag{9}$$

where E_l and ϕ_l (the locked phase) are real constants. By insertion into (8) we obtain

$$E_l^2 = \frac{\kappa^2}{\Gamma_l^2 + \alpha^2(\Gamma_l + \kappa)^2} E_s^2 \tag{10}$$

using $\Delta\omega_s = -\alpha\kappa/\tau_{in}$ from (7a). Also $\Gamma_l = \Gamma(N_l)$, where N_l is the constant carrier density and Γ is the parameter defined by

$$\Gamma(N) = \tfrac{1}{2}\tau_{in}G_N(N - N_{th}). \tag{11}$$

From (4) we obtain $(dN/dt = 0)$

$$J - \frac{N_l}{\tau_s} = G_N(N_l - N_o)|E_l|^2 \tag{12a}$$

or by use of (10) and (11)

$$\left(\frac{J}{J_{th}} - 1\right)\frac{N_{th}}{\tau_s} - \frac{2\Gamma_l}{G_N\tau_{in}\tau_s}$$
$$= \left(\frac{1}{\tau_p} + \frac{2\Gamma_l}{\tau_{in}}\right)\frac{\kappa^2 E_s^2}{\Gamma_l^2 + \alpha^2(\Gamma_l + \kappa)^2}. \tag{12b}$$

From (12b) we determine the possible quasi-stationary solutions with respect to Γ_l. In Fig. 2 the solutions are determined as the intersection points between the straight line on the left-hand side of (12b) and the curve on the

TABLE I
LASER PARAMETERS AND THEIR NUMERICAL VALUES

Parameter	Symbol	Value
Gain coefficient	G_N	$1.1 \cdot 10^{-12} \, m^3 \cdot s^{-1}$
Transparency carrier density	N_o	$1.1 \cdot 10^{24} \, m^{-3}$
Carrier lifetime	τ_s	0.5 ns
Photon lifetime	τ_p	2 ps
Laser cavity roundtrip time	τ_{in}	8 ps
Linewidth enhancement factor	α	6
Active region volume	V	$1 \cdot 10^{-16} \, m^3$
Spontaneous emission factor	n_{sp}	3.42
Curvature of gain curve	$G_{\omega\omega}$	$-1.6 \cdot 10^{-15} \, s$
Shift of gain peak	ω_{RN}	$2.12 \cdot 10^{-11} \, m^3 \cdot s^{-1}$

Fig. 3. Total photon numbers I_a, I_b, I_c shown as a function of normalized bias current J/J_{th} for $\kappa = 0.15$. I_{sol} denotes the stationary solution for the solitary laser. Unstable solutions are indicated by dashed curves.
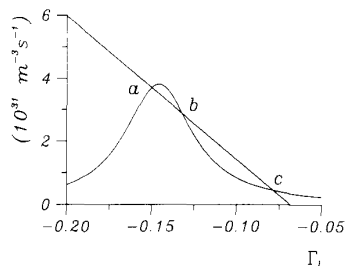

Fig. 2. Stationary solutions by constant injection of stationary feedback field. Graphical solution of (12b) for $J/J_{th} = 0.99$, $\kappa = 0.15$. Three solutions: $E_l = E_{a,b,c}$, where $E_a = E_s$.

Fig. 4. Real part of the eigenvalues λ_l for the stationary solutions I_l of Fig. 3. ———: $l = a$, $\cdots$: $l = b$, ---: $l = c$.

right-hand side of (12b) for fixed bias current $J/J_{th} = 0.99$. Three solutions (Γ_l, E_l), $l = a, b, c$, are obtained, where $(\Gamma_a, E_a) = (-\kappa, E_s)$ is the usual stationary solution.

In Fig. 3 the photon numbers $I_l = VE_l^2$, $l = a, b, c$, are shown as a function of bias current, and we have included the stationary solution for the solitary laser, $I = I_{sol}$.

The dynamic stability of the stationary solutions shown in Fig. 3 need to be investigated. This is accomplished by separation of (8) into equations for the real amplitude $E_o(t)$ and the real phase $\phi(t)$, $E(t) = E_o(t) \exp[j\phi(t)]$, and allowing for small fluctuations around the stationary state; $E_o(t) = E_l + \delta E(t)$, $\phi(t) = \phi_l + \Delta\omega_s t + \delta\phi(t)$, $N(t) = N_l + \delta N(t)$. Letting $\overline{\delta Y} = (\delta E, \delta\phi, \delta N)^T$ we obtain to first order a set of equations $d/dt(\overline{\delta Y}) = \overline{M}_l \cdot \overline{\delta Y}$, where $\overline{M}_l$ is a 3 × 3 matrix. The condition for first-order dynamic stability of the stationary solution denoted by subscript l is that all three eigenvalues λ_l of $\overline{M}_l$ are located in the left half of the complex λ-plane.

In Fig. 4 the real parts of the eigenvalues λ_l are depicted as a function of the bias current for the stationary solutions a, b, and c of Fig. 3. From the figure it is seen that the stationary solution a (solid curves) is always stable, the intermediate solution b (dotted curves) is always unstable, and c (dashed curves) is stable for $J/J_{th} \leq 1.0$. The point where solution c becomes unstable corresponds by comparison with Fig. 3 to the point where I_{sol} intersects I_c. Beyond this value of the bias current the stationary solution c loses stability in favor of a limit cycle solution oscillating around the solitary level I_{sol}, with a pulsation frequency approximately given by the beat frequency between the dominant external cavity mode and the solitary solution. A solution of this kind was also rec-
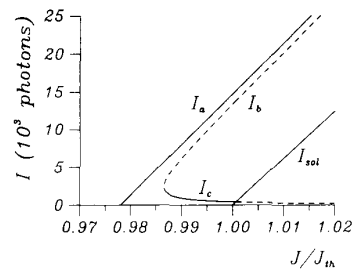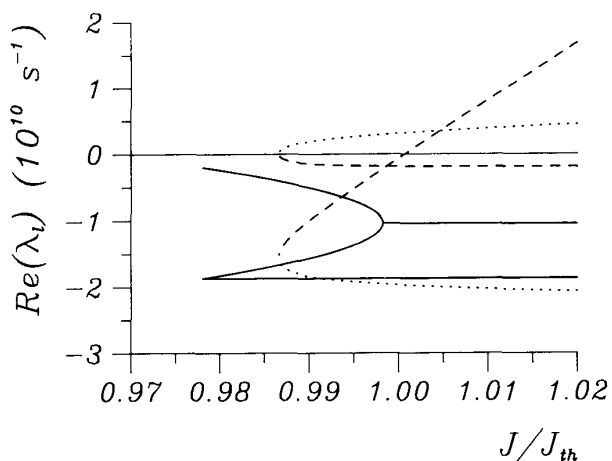
ognized in [32]. Fig. 5 shows the limit cycle in the normalized (I, N)-plane for $J/J_{th} = 1.02$. In the adiabatic approximation $(dN/dt \simeq 0)$ the appearance of instability for $J \simeq J_{th}$ may be illustrated by considering (8) as an equation for a particle in a static potential and exposed to an external driving force. For $J \simeq J_{th}$ the origin $(E = 0)$ becomes a potential maximum instead of a minimum (Hopf bifurcation).

For the stable solution a, three different real eigenvalues are found for $J \leq J_{th}$. Two of these merge (cf. Fig. 4) and acquire imaginary parts at $J \simeq J_{th}$, thus defining a characteristic relaxation oscillation frequency. For the unstable solution b, the upper branch in Fig. 4 corresponds to an eigenvalue on the real positive axis, while the lower branch gives the real part of two complex conjugate eigenvalues. The branch that crosses the axis Re $(\lambda_l) = 0$ in Fig. 4 arises from a set of complex conjugate eigenvalues for solution c, while the other (dashed) branch corresponds to a real eigenvalue.

The presence of another stable solution I_c besides I_s ($I_s = I_a$) permits a bistable behavior. The power drop seen in Fig. 1 can thus be understood as a noise-induced switching between the two states. The switching mechanism, which exists despite the just demonstrated first-order stability, will be discussed below, but we shall first comment on the qualitative features of Figs. 3 and 4.
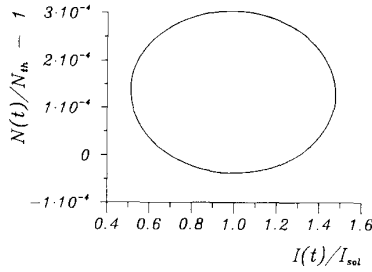
Fig. 5. Limit cycle solution in the normalized (I, N)-plane for $J/J_{th} = 1.02$, $\kappa = 0.15$.

Fig. 3 shows that bistability is absent below a critical bias current J_{bs} ($\simeq 0.987 \cdot J_{th}$), where $J'_{th} < J_{bs} < J_{th}$. For $J < J_{bs}$ we then expect $\bar{I} = I_s$, where bar denotes time averaging, since no other quasi-stationary solution exists in this current range. For $J_{bs} < J \lesssim J_{th}$, however, dynamical switching to another stable state $I_c < I_s$ could be possible, which would lead to an average photon number $\bar{I} < I_s$. This relates the kink in the light–current characteristic to the emergence of bistability. Above threshold for the solitary laser the bistable switching is strongly influenced by the spontaneous emission noise as we shall see in Section III.

Having demonstrated the linear stability of the stationary solution a, the presence of some kind of higher order instability is necessary in order to make possible a noise-induced transition from state a to state c. Such an instability was found by Henry and Kazarinov [17] and shown to be equivalent to the possibility of a particle crossing a potential barrier when acted upon by random forces (spontaneous emission events). An expression for the mean time t_I for the transition to occur was obtained by an approximate solution of the associated Fokker–Planck equation. The expression they obtained for t_I is in our notation

$$t_I = \frac{\tau_s x}{1 + x} \exp \left\{ \frac{8 V \tau_p^2 \kappa^3 (1 + x)^3}{3 \alpha^4 G_N n_{sp} \tau_{in}^3} \right\} \qquad (13)$$

with

$$x = \frac{\kappa J_{th}}{G_N N_{th} \tau_{in} (J - J'_{th})} \qquad (14)$$

and is derived for the detuning $d = 0$ and $\kappa \gtrsim 0.01$ (see [17]). In (13) n_{sp} is the spontaneous emission factor. t_I is infinite for $J = J'_{th}$ (i.e., the laser is stable) but decreases with J for $J > J'_{th}$. The decrease is very steep until $x \ll 1$, after which t_I decreases proportionally to x. From t_I one can estimate the average intensity as a function of bias current, and in [17] this was shown to reproduce the experimental results [10] for the kinked light–current characteristics. The dependence of t_I on the detuning d was not investigated in [17], but experiments [12], [33] and theory [9] show a critical dependence, in particular for lower levels of feedback. We shall return to this discussion in Section IV-B.

III. ITERATIVE DESCRIPTION

In the preceding section we did not take into account the spontaneous emission noise. Qualitatively, an average spontaneous emission rate into the lasing mode gives rise to a narrow infinitely high peak in Fig. 2 at $\Gamma_I = 0$ (see, e.g., [28]), which results in a continuous connection of the stable branches I_c and I_{sol} in Fig. 3. In the present section we further pursue this subject and its implications for the intensity buildup by the addition of a Langevin noise term to the RHS of (1).

The complex Langevin noise term is represented by [9]

$$F_E(t) = \frac{1}{\sqrt{V}} \sum_i e^{j\Theta_i} \delta(t - t_i) \qquad (15)$$

where the summation is over all randomly occurring spontaneous emission events into the lasing mode. The phases Θ_i of the individual contributions in (15) are uncorrelated.

Defining the Fourier transform of $E(t)$ by

$$\mathcal{E}(\omega - \omega_o) = \int_{-\infty}^{\infty} E(t) \exp \left[-j(\omega - \omega_o) t \right] dt \qquad (16)$$

we obtain from (1)

$$\mathcal{E}(\Delta\omega) = \frac{\kappa e^{-j\omega\tau} \mathcal{E}^i(\Delta\omega) + F(\Delta\omega)}{j\Delta\omega\tau_{in} - (1 + j\alpha)\Gamma} \qquad (17)$$

where $\Delta\omega = \omega - \omega_o$, $F(\Delta\omega)$ is the transform of the Langevin term $F_E(t)$, and the transform stemming from the delayed feedback of (1) has been indicated by superscript i. In deriving (17) we have assumed $N(t)$ to be clamped at some value. From (17) we obtain by squaring and ensemble averaging

$$S(\Delta\omega) = \frac{\kappa^2 S^i(\Delta\omega) + R\tau_{in}^2 V^{-1}}{(\Delta\omega\tau_{in} - \alpha\Gamma)^2 + \Gamma^2} \qquad (18)$$

where

$$S(\Delta\omega) = \left\langle \left| \mathcal{E}(\omega - \omega_o) \right|^2 \right\rangle \qquad (19)$$

is the field power spectrum and similarly for $S^i(\Delta\omega)$. The ensemble average indicated by $\langle \ \rangle$ includes an average over time; see [19] for details. In deriving (18) we have neglected correlations between $\mathcal{E}^i(\Delta\omega)$ and $F(\Delta\omega)$, and the last term of the numerator expresses the white spectrum $\langle | F(\Delta\omega) |^2 \rangle$ of the Langevin term. The rate of spontaneous emission into the lasing mode is taken as [30]

$$R = n_{sp} G(N_{th}). \qquad (20)$$

Equation (18) expresses the laser spectrum in response to an externally injected field with spectrum $S^i(\Delta\omega)$, where, however, the carrier density level still has to be determined. From (4) we find

$$J - \frac{N}{\tau_s} = G_N (N - N_o) I(\Gamma) \cdot V^{-1} \qquad (21a)$$

where the total photon number $I(\Gamma)$ is expressed by the

integrated field power spectrum

$$I(\Gamma)V^{-1} = \frac{1}{2\pi} \int_{-\infty}^{\infty} S(\Delta\omega)\,d(\Delta\omega). \quad (21b)$$

Given $S^i(\Delta\omega)$ the resulting field power spectrum and carrier density level are found by solution of (18) and (21). A generalized form of these equations has been presented in [29].

The stationary spectrum $S(\Delta\omega) = S^i(\Delta\omega) = S_s(\Delta\omega)$ is found from (18)

$$S_s(\Delta\omega) = \frac{R\tau_{in}^2 V^{-1}}{\left(\Delta\omega\tau_{in} - \alpha\Gamma_s\right)^2 + \Gamma_s^2 - \kappa^2} \quad (22)$$

with which (21) takes the specific form

$$J - \frac{N_s}{\tau_s} = G_N(N_s - N_o)\frac{R\tau_{in}}{2V\sqrt{\Gamma_s^2 - \kappa^2}} \quad (23)$$

having a single solution $\Gamma_s = \Gamma(N_s)$ close to $-\kappa$.

The spectrum (22) is, of course, only a crude approximation, as the effect of carrier density fluctuations and the coherence between the Langevin noise and the resulting field have been neglected. It suffices, however, for our investigation of the "global" dynamics, which includes large excursions from the stationary state.

Upon external injection of a field with spectrum $S^i(\Delta\omega) = S_s(\Delta\omega)$ we obtain a carrier density N obeying

$$J - \frac{N}{\tau_s} = G_N(N - N_o)\frac{1}{2\pi}$$

$$\cdot \int_{-\infty}^{\infty} \frac{\kappa^2 S_s(\Delta\omega) + R\tau_{in}^2 V^{-1}}{\left(\Delta\omega\tau_{in} - \alpha\Gamma\right)^2 + \Gamma^2}\,d(\Delta\omega) \quad (24)$$

which is equivalent to (12) except for the inclusion of spontaneous emission noise. Here we also obtain two solutions besides $N = N_s$ with a possibility of a noise-induced switching to the higher (stable) one previously labeled c. Introducing the shift at a given time we determine the subsequent evolution of carrier density and laser spectra by an iterative solution of (18) and (21).

Defining N_n and $S_n(\Delta\omega)$ to be carrier density and field power spectrum in the time interval
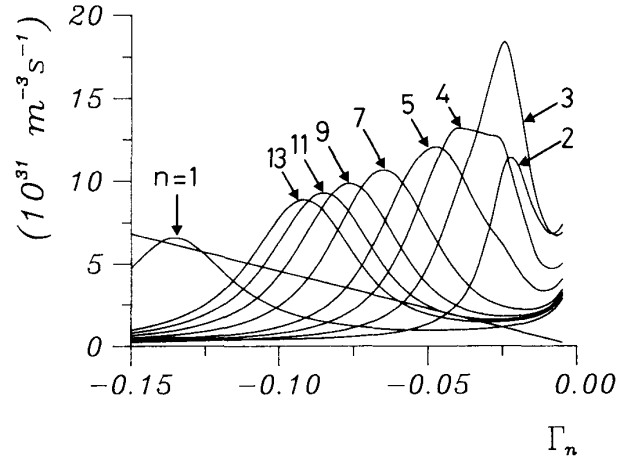
$$n\tau < t < (n + 1)\tau \quad (25)$$

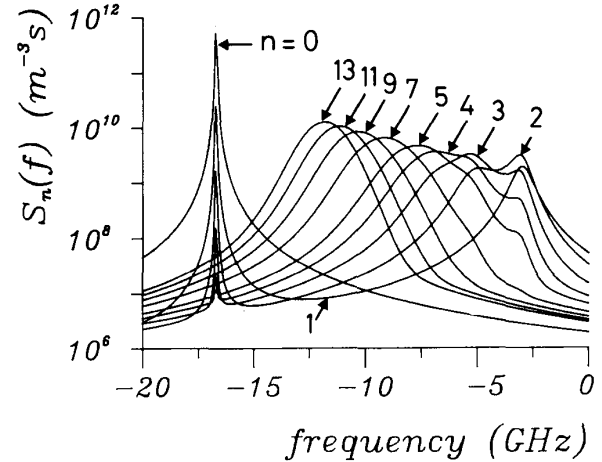(18) and (21) take the iterative form

$$J - \frac{N_n}{\tau_s} = G_N(N_n - N_o)\frac{1}{2\pi}\int_{-\infty}^{\infty} S_n(\Delta\omega)\,d(\Delta\omega)$$

$$\quad (26a)$$

$$S_n(\Delta\omega) = \frac{\kappa^2 S_{n-1}(\Delta\omega) + R\tau_{in}^2 V^{-1}}{\left(\Delta\omega\tau_{in} - \alpha\Gamma_n\right)^2 + \Gamma_n^2}, \quad n = 1, 2, \cdots,$$

$$\quad (26b)$$

where $\Gamma_n = \Gamma(N_n)$. The iteration starts with $S_o(\Delta\omega) = S_s(\Delta\omega)$, and for $t = \tau$ we choose the higher solution, $\Gamma_n = \Gamma_1$, instead of the stationary solution, $\Gamma_n = \Gamma_o \equiv \Gamma_s$.

(a)

frequency (GHz)

(b)

Fig. 6. Solution of the iterative multimode equations corresponding to (26) for $\kappa = 0.15$, $J = J_{th}$, and $n = 1$–13. (a) Graphical solution of (26a). (b) Corresponding spectra (26b) for the central mode as a function of frequency, $f = (\omega - \omega_o)/2\pi$.

Fig. 6 depicts the graphical solution of (26a) and the resulting field power spectrum (26b) for $\kappa = 0.15$, $J = J_{th}$, and $n = 0$–13. In Fig. 6(a) the curves tend to infinity for $\Gamma_n \to 0$. To keep the discussion simple we have only derived (26) for the single-mode case. However, the results of Figs. 6–8 are actually derived from a generalized form of (26) given in [29, eqs. (64) and (65)]. The latter include multimode effects and also apply to strong feedback and to DFB lasers. No basic feature of (26) is changed by including multimode effects, but it permits a closer comparison with our multimode traveling wave simulations.

Fig. 6(a) shows that after the initial switching (on the curve labeled 1, i.e., the RHS of (26a) as a function of Γ_n for $n = 1$) from the lower intersection point $\Gamma_n = \Gamma_s \equiv \Gamma_o$ to the higher intersection point $\Gamma_n = \Gamma_1$, only one solution exists for $n = 2$–10. This means that bistability is absent during the initial buildup, and no switching is possible. For $n = 11$, bistability is restored and a noise-induced switching becomes possible again. The spectral
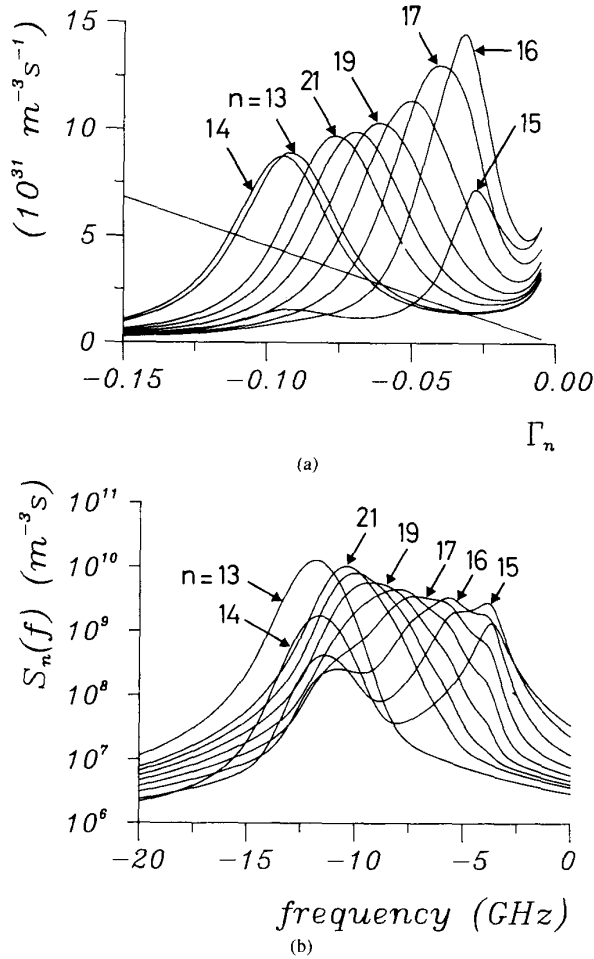
(a)

frequency (GHz)

(b)

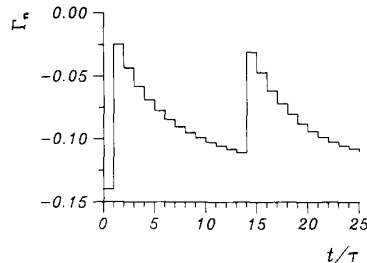Fig. 7. As Fig. 6 but for $n = 13$-21. See text for details.

Fig. 8. Variation of $\Gamma_n = \frac{1}{2} \tau_{in} G_N (N_n - N_{th})$ for Figs. 6 and 7, $n = 0$-21.

changes shown in Fig. 6(b) mainly consist of the formation of a new peak at a frequency slightly below the solitary value followed by a gradual broadening and shift towards lower frequencies.

From both Fig. 6(a) and (b) it is seen that the stationary state has not yet been recovered, when bistability occurs. In Fig. 7 we have induced a switching at $n = 14$, i.e., the initial, very narrow spectrum ($n = 0$) of Fig. 6(b) is actually replaced with the much broader spectrum at $n = 13$. This leads to additional overlap of the high and low

frequency peaks. At $n = 23$ it is found that the spectrum is close to that of $n = 13$, and bistability occurs. Thus we have obtained a closed loop which qualitatively describes the dynamics of the low-frequency fluctuations, where, however, the actual time delays between the occurrence of bistability and the switching are stochastic.

The results of Figs. 6 and 7 are summarized in Fig. 8, where the variation of Γ_n (or, equivalently, N_n) is shown.

IV. NOISE SIMULATIONS

A. The Multimode Traveling Wave Model

For computer simulations we have adopted a multimode traveling wave model as originally proposed in [16] and developed further in [29]. In [29] this model is shown to be a generalization of the rate equation of Lang and Kobayashi [1]. Some simple approximations render the model onto the form of a set of difference equations, which are readily solved on a computer. We will not give a detailed derivation of the model but merely present the equations, which are intuitively obvious.

The slowly-varying complex envelope of the mth longitudinal laser cavity mode evolves according to

$$E_m(t + \tau_{in}) = \exp \left\{ \frac{1}{2} \tau_{in} \left[(1 + j\alpha) G_N(N - N_{th}) \right. \right.$$
$$\left. + G_2(\omega_m, N) \right] \}$$
$$\cdot \left\{ E_m(t) + \kappa \exp (-j\Omega_m\tau) E_m(t - \tau) \right\}$$
$$+ \Delta F_E(\tau_{in}). \tag{27}$$

The $(2M + 1)$ longitudinal angular mode frequencies of the solitary laser are

$$\Omega_m = \omega_o + m\Delta\Omega, \quad m = 0, \pm 1, \cdots, \pm M \tag{28a}$$

where $\Delta\Omega$ is the mode spacing

$$\Delta\Omega = \frac{2\pi}{\tau_{in}}. \tag{28b}$$

The oscillating frequency of the mth mode is

$$\omega_m(t) = \Omega_m + \dot{\phi}_m(t) \tag{29}$$

and $E_m(t) = |E_m(t)| \exp [j\phi_m(t)]$. The frequency dependence of the gain curve is

$$G(\omega, N) = G_N (N - N_o) + \frac{1}{2} G_{\omega\omega} (\omega - \omega_R (N))^2$$
$$= G(N) + G_2(\omega, N) \tag{30a}$$

where $G_{\omega\omega} = \partial^2 G/\partial\omega^2$ (<0) is a constant, and the peak of the gain curve shifts with carrier density as

$$\omega_R (N) = \omega_{R0} + \omega_{RN} (N - N_{th}) \tag{30b}$$

where $\omega_{RN} = \partial\omega_R/\partial N$ is a constant. For the solitary laser we assume the gain peak to coincide with one of the longitudinal modes, i.e., $\omega_{R0} = \omega_o$.

$\Delta F_E (\tau_{in})$ denotes the integrated noise density (15). If the mean number of spontaneous emission events occurring in a time interval of length τ_{in} is large, $R \cdot \tau_{in} \gg 1$, the real and imaginary parts of ΔF_E may be generated

from independent normal distributions with zero mean and standard deviations [9]

$$\sigma = \left(\frac{R\tau_{\text{in}}}{2V}\right)^{1/2}. \quad (31)$$

We take R to be mode-independent.

In the multimode case the rate equation for the carrier density (4) is replaced by

$$\frac{d}{dt} N(t) = J - \frac{N(t)}{\tau_s} - \sum_m G(\omega_m, N) |E_m(t)|^2 \quad (32)$$

where the summation is over the mode numbers $m = -M$, $\cdots$, M, $I_m = V \cdot |E_m|^2$ is the number of photons in the mth mode, and $I = \Sigma_m I_m$ is the total photon number. By this the longitudinal modes are assumed to interact only via the reservoir of carriers.

The evolution of carrier density is calculated by application of a second-order Taylor expansion

$$N(t + \tau_{\text{in}}) \cong N(t) + \frac{dN}{dt}\bigg|_t \tau_{\text{in}} + \frac{1}{2} \frac{d^2N}{dt^2}\bigg|_t (\tau_{\text{in}})^2. \quad (33)$$

The first-order derivative is given by (32), and the second-order derivative is found by differentiation. This includes calculation of dE_m/dt, which is obtained from (27) by a first-order expansion of the exponential and approximating $E_m(t + \tau_{\text{in}}) \cong E_m(t) + \tau_{\text{in}} \cdot dE_m/dt$. This essentially corresponds to using the rate equation expression for the derivative of the electrical field.

In order to obtain a numerically stable scheme, where the solution is advanced in steps of τ_{in}, it has proved necessary to include the second-order term in (33). At low feedback levels we obtain good agreement between numerically obtained spectra and a small-signal model based on the single-mode rate equations.

B. Results

In this section we present some specific examples of simulations with the traveling wave model. If nothing else is mentioned we have used seven longitudinal modes, a feedback level of $\kappa = 0.15$ (-16.5 dB), an external cavity roundtrip time $\tau = 10$ ns (corresponding to a cavity length of 1.5 m) and set the (noise-free, see [9]) detuning to zero. The remaining parameters are specified in Table I. Qualitatively similar results were obtained for an external cavity length of 60 cm and do not seem to depend critically on the specific cavity length in this long cavity limit; see [33]. The performance of an averaging procedure simulating the limited bandwidth of a physical detection process is essential for the identification of a LFF-component out of the otherwise very noisy-looking time evolution. We have therefore in all simulations performed a running average over 100 points spaced by τ_{in}, roughly corresponding to a detector bandwidth of 1.25 GHz.

First, we show a number of results for the state corresponding to Fig. 1, i.e., $J = J_{\text{th}}$.

Fig. 9 shows the variation of carrier density in one of the fundamental "periods" consisting of (here) approxi-
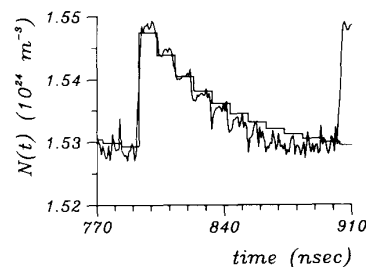

Fig. 9. Simulated time evolution of carrier density (noisy trace) compared with iterative solution. $J = J_{\text{th}}$, $\kappa = 0.15$, $\tau = 10$ ns.

mately 11 external cavity roundtrip periods and the corresponding (horizontally shifted) variation of N_n from Fig. 8 for $n = 12$–25. The curves compare qualitatively well, but the iteratively determined step curve tends to show too strong saturation. This is probably due to the neglection of the carrier density fluctuations and relaxation oscillations, which tend to broaden the spectra and thereby provide an additional frequency-pulling effect.

Fig. 10 depicts the result of sampling the field power spectrum in some of the (discrete) steps of Fig. 9. The spectrum labeled $n' = 0$ corresponds to the quasi-stationary state just before the steep increase of $N(t)$ at $t \cong 795$ ns, and $n' = 1$–3 labels the spectra in the following steps of length τ. The spectra were calculated in the usual way [9] and ranged over a time interval of total length 8.2 ns with spacing τ_{in}. This gives a resolution of 120 MHz in the frequency domain and an upper frequency of 62.5 GHz. The resulting spectra were averaged over 15 adjacent points. The simulated spectra show the same general features as obtained in Fig. 7(b), including the formation of a double peak and a subsequent shift towards lower frequencies. However, as expected the spectra of Fig. 10 are considerably broader than those of Fig. 7(b). The dynamic shift of a broad spectrum towards lower frequencies was observed experimentally in [15] for a grating cavity.

In Fig. 11 we show the simulated average multimode spectrum. It is in qualitative agreement with the broad multimode spectrum observed experimentally [10], [13]. The asymmetry of the spectrum is due to the (dynamic) shift of the gainpeak towards lower frequencies. The anomalous interaction mechanism of Bogatov et al. [26] arising from intraband relaxation will cause a similar asymmetry [34], but that effect is not included in the model. It does, however, include the anomalous interaction due to interband relaxation (τ_s). This gives rise to an asymmetry in the spectrum on the scale of the external cavity modes (cf. [9, Figs. 16 and 17] and [22, Figs. 3a–d]) but has no (or little) influence on LFF.

Next, we consider the effect of varying the bias current with fixed external cavity conditions $\kappa = 0.15$ and $\tau = 10$ ns. Fig. 12 shows the evolution of total photon number $I(t)$ normalized by the stationary (single-mode traveling wave) solution I_s for six different bias currents: $J/J_{\text{th}} = 0.9825$, 0.99, 1.00, 1.01, 1.02, and 1.30. The simulations start from the stationary single-mode solutions, and
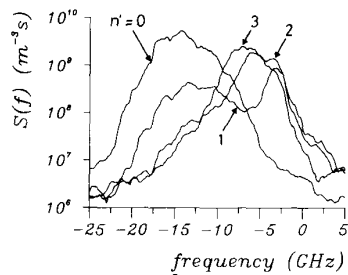
Fig. 10. Simulated field power spectra for the central mode in different steps of Fig. 9. $n' = 0$ denotes the state just before the steep increase of $N(t)$ at $t \cong 795$ ns.
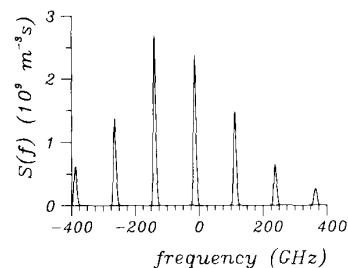

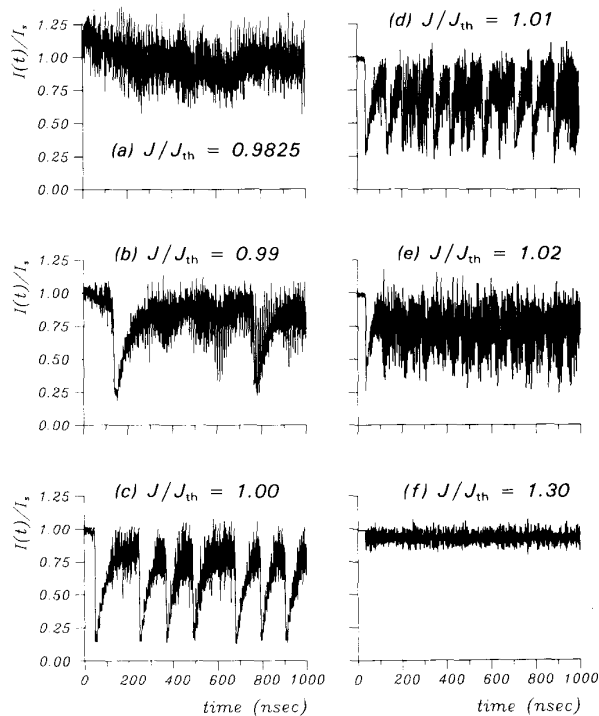Fig. 11. Time-averaged field power spectrum. $J = J_{\text{th}}$, $\kappa = 0.15$, $\tau = 10$ ns.

Fig. 12. Simulated time evolution of normalized total photon number for different bias currents J/J_{th}. $\kappa = 0.15$, $\tau = 10$ ns.
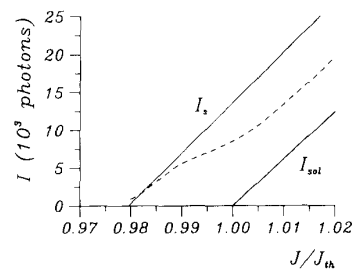
Fig. 13. Light–current characteristics for stationary solutions with (I_s) and without (I_{sol}) feedback, and for simulated solution (dashed curve). $\kappa = 0.15$, $\tau = 10$ ns.

Fig. 14. As Fig. 12(c) but for $t > 100$ ns the noise generator is turned off.

the occurrence of a kink in the light–current characteristics, which is in qualitative agreement with experimental observations [10], [13], [33]. Comparison with the time series of Fig. 12 reveals the kink to be due to a decrease of the LFF period with increasing bias current and an associated increase of the pulling of average intensity from the stationary value. Well-above threshold [see Fig. 12(f)] the LFF cannot be time resolved and the total photon number is observed to fluctuate seemingly randomly between the stationary value with feedback and the solitary value. This results in an average intensity which is nearly midway between the curves of (optimum) coherent feedback and no feedback.

The mean frequency of the intensity drops gives the position of the peak in the intensity noise spectrum due to the LFF. It is seen to increase from about 7 MHz in Fig. 12(c) to about 17 MHz in Fig. 12(e), which is in qualitative agreement with experiments, see [12] and [10, Fig. 5].

The mean time t_l for the first intensity drop to occur can be calculated from (13) and (14). If we insert the bias currents of Fig. 12(a)–(f) we find $t_l = 6.9 \cdot 10^{16}$ s, 6.4 μs, 22 ns, 4.2 ns, 1.9 ns, and 81 ps, respectively. Except for Fig. 12(a) and (b) the first intensity drop is seen to occur after 30–50 ns, and there is no sign of the dramatic decrease expected from the values of t_l. A similar delay (20–40 ns) for the first intensity drop is observed when using only a single longitudinal mode in the simulations, so the reason for the discrepancy is not that t_l is derived for the single-mode case, while we are using a multimode model. However, the inclusion of several longitudinal modes has been found to have a significant stabilizing effect on the LFF. The staircases of intensity buildup are much more regular when more modes are included.

at $t = 0$ we switch on the noise generator. In Fig. 13 we have plotted the light–current characteristics obtained from the average intensities of Fig. 12 and additional runs in the range $0.98 \leqq J/J_{\text{th}} \leqq 1.02$. Fig. 13 demonstrates
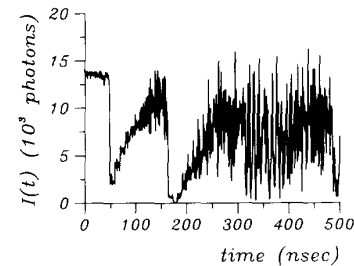
Also the spontaneous emission noise has a smoothing effect on the intensity fluctuations. In Fig. 14 we show a simulation with the parameters of Fig. 12(c), but for $t >$ 100 ns (i.e., after the first power drop) we have turned off the noise generator. We find that the LFF seem to persist, but there is a marked increase in the high-frequency intensity noise. This self-generated noise seems to indicate that the motion takes place on a chaotic attractor. A decisive proof may, however, require a computation of the Lyapunov exponents [18], [35].

V. CONCLUSION

We have presented a detailed investigation of the dynamics of low-frequency fluctuations, which occur in a semiconductor laser biased near threshold and exposed to moderate amounts of optical feedback.

Simulations with a noise-driven multimode traveling wave model, which permits inexpensive computations, have been demonstrated to reproduce the experimentally observed pattern of LFF. Calculation of the average intensities from the simulated time-series further demonstrates the experimentally observed kink in the light–current characteristics to be contained in the simulation model. The kink is due to a rapid decrease of the LFF period with increasing bias current.

We have derived an approximate set of iterative equations which relates the carrier density and the power spectrum, for one time step of a length equal to the external cavity roundtrip period τ to the "driving" spectrum of the previous step. By this procedure the LFF are understood to occur as a result of bistability, which permits a noise-induced switching to a low-power state. From this state the intensity builds up again in steps of of length τ. During the initial buildup bistability is absent, but is restored after typically 10 τ, making a noise-induced switching possible again. This dynamical behavior, we believe, explains the LFF.

The observed stability for bias currents below the kink has been explained as being due to the absence of bistability below a certain critical value of the bias current. Experiments [10] indicate that the LFF are suppressed at very high levels of optical feedback obtained by AR-coating the laser facet facing the external cavity. In a similar way we expect this to be explicable by the absence of bistability beyond a critical high feedback level.

In [10], [17] the experimentally observed very broad laser line is seen merely as a result of the frequency chirp associated with the LFF. From simulations we find that there is a significant pulling of the average oscillation frequency during one "period" of the LFF but also that spectra sampled at different times during this period show a comparable broadening. This is in qualitative agreement with results obtained by the approximate iterative equations.

The question of chaotic dynamics has not been directly addressed. We have, however, found that turning off the noise generator does not lead to the disappearance of LFF, but instead to an increase of the high-frequency in-

tensity noise. This might indicate that the motion takes place on a chaotic attractor. Deterministic chaos may be distinguished quantitatively from regular motion by computation of the spectrum of Lyapunov exponents [18], [35]. Such work is in progress and will be reported elsewhere.

REFERENCES

[1] R. Lang and K. Kobayashi, "External optical feedback effects on semiconductor injection laser properties," IEEE J. Quantum Electron., vol. QE-16, pp. 347–355, Mar. 1980.
[2] K. Kikuchi and T. Okoshi, "Simple formula giving spectrum-narrowing ratio of semiconductor-laser output obtained by optical feedback," Electron. Lett., vol. 18, pp. 10–11, Jan. 1982.
[3] E. Patzak, H. Olesen, A. Sugimura, S. Saito, and T. Mukai, "Spectral linewidth reduction in semiconductor lasers by an external cavity with weak optical feedback," Electron. Lett., vol. 19, pp. 938–940, Oct. 1983.
[4] L. Goldberg, H. F. Taylor, A. Dandridge, J. F. Weller, and R. O. Miles, "Spectral characteristics of semiconductor lasers with optical feedback," IEEE J. Quantum Electron., vol. QE-18, pp. 555–564, Apr. 1982.
[5] F. Favre, D. Le Guen, and J. C. Simon, "Optical feedback effects upon laser diode oscillation field spectrum," IEEE J. Quantum Electron., vol. QE-18, pp. 1712–1717, Oct. 1982.
[6] J. Mark, E. Bødtker, and B. Tromborg, "Measurement of Rayleigh backscatter-induced linewidth reduction," Electron. Lett., vol. 21, pp. 1008–1009, Oct. 1985.
[7] R. O. Miles, A. Dandridge, A. B. Tveten, H. F. Taylor, and T. G. Giallorenzi, "Feedback-induced line broadening in cw channel-substrate planar laser diodes," Appl. Phys. Lett., vol. 37, pp. 990–992, Dec. 1980.
[8] D. Lenstra, B. H. Verbeek, and A. J. den Boef, "Coherence collapse in single-mode semiconductor lasers due to optical feedback," IEEE J. Quantum Electron., vol. QE-21, pp. 674–679, June 1985.
[9] H. Olesen, J. H. Osmundsen, and B. Tromborg, "Nonlinear dynamics and spectral behavior for an external cavity laser," IEEE J. Quantum Electron., vol. QE-22, pp. 762–773, June 1986.
[10] H. Temkin, N. A. Olsson, J. H. Abeles, R. A. Logan, and M. B. Panish, "Reflection noise in index-guided InGaAsP lasers," IEEE J. Quantum Electron., vol. QE-22, pp. 286–293, Feb. 1986.
[11] M. Ito and T. Kimura, "Oscillation properties of AlGaAs DH lasers with an external grating," IEEE J. Quantum Electron., vol. QE-16, pp. 69–77, Jan. 1980.
[12] M. Fujiwara, K. Kubota, and R. Lang, "Low-frequency intensity fluctuation in laser diodes with external optical feedback," Appl. Phys. Lett., vol. 38, pp. 217–220, Feb. 1981.
[13] R. Ries and F. Sporleder, "Low-frequency instabilities of laser diodes with optical feedback," in Proc. 8th ECOC, Cannes, France, Sept. 1982, pp. 285–290.
[14] T. Morikawa, Y. Mitsuhashi, J. Shimada, and Y. Kojima, "Return-beam-induced oscillations in self-coupled semiconductor lasers," Electron. Lett., vol. 12, pp. 435–436, Aug. 1976.
[15] C. Risch and C. Voumard, "Self-pulsation in the output intensity and spectrum of GaAs-AlGaAs cw diode lasers coupled to a frequency selective external optical cavity," J. Appl. Phys., vol. 48, pp. 2083–2085, May 1977.
[16] F. Sporleder, "Travelling wave line model for laser diodes with external optical feedback," in Proc. URSI Int. Symp. Electromagnet. Theory, Santiago de Compostela, Spain, Aug. 1983, pp. 585–588.
[17] C. H. Henry and R. F. Kazarinov, "Instability of semiconductor lasers due to optical feedback from distant reflectors," IEEE J. Quantum Electron., vol. QE-22, pp. 294–301, Feb. 1986.
[18] J. D. Farmer, "Chaotic attractors of an infinite-dimensional dynamical system," Physica, vol. 4D, pp. 366–393, 1982.
[19] P. Spano, S. Piazzolla, and M. Tamburrini, "Theory of noise in semiconductor lasers in the presence of optical feedback," IEEE J. Quantum Electron., vol. QE-20, pp. 350–357, Apr. 1984.
[20] B. Tromborg, J. H. Osmundsen, and H. Olesen, "Stability analysis for a semiconductor laser in an external cavity," IEEE J. Quantum Electron., vol. QE-20, pp. 1023–1032, Sept. 1984.
[21] R. Müller and P. Glas, "Bistability, regular self-pulsing, and chaos in lasers with external feedback," J. Opt. Soc. Amer. A, vol. 2, pp. 184–192, Jan. 1985.

[22] T. Mukai and K. Otsuka, "New route to optical chaos: Successive-subharmonic-oscillation cascade in a semiconductor laser coupled to an external cavity," *Phys. Rev. Lett.*, vol. 55, pp. 1711-1714, Oct. 1985.

[23] K. Otsuka and T. Mukai, "Asymmetrical coupling, locking and chaos in a compound cavity semiconductor laser," in *Proc. SPIE Symp. Opt. Chaos*, Quebec, P.Q., Canada, June 1986, pp. 122-129.

[24] Y. Cho and T. Umeda, "Observation of chaos in a semiconductor laser with delayed feedback," *Opt. Commun.*, vol. 59, pp. 131-136, Aug. 1986.

[25] K. A. Shore, "Non-linear dynamics and chaos in semiconductor laser devices," *Solid-State Electron.*, vol. 30, pp. 59-65, 1987.

[26] A. P. Bogatov, P. G. Eliseev, and B. N. Sverdlov, "Anomalous interaction of spectral modes in a semiconductor laser," *IEEE J. Quantum Electron.*, vol. QE-11, pp. 510-515, July 1975.

[27] F. Mogensen, H. Olesen, and G. Jacobsen, "Locking conditions and stability properties for a semiconductor laser with external light injection," *IEEE J. Quantum Electron.*, vol. QE-21, pp. 784-793, July 1985.

[28] C. H. Henry, N. A. Olsson, and N. K. Dutta, "Locking range and stability of injection locked 1.54 μm InGaAsP semiconductor lasers," *IEEE J. Quantum Electron.*, vol. QE-21, pp. 1152-1156, Aug. 1985.

[29] B. Tromborg, H. Olesen, X. Pan, and S. Saito, "Transmission line description of optical feedback and injection locking for Fabry–Perot and DFB lasers," *IEEE J. Quantum Electron.*, vol. QE-23, pp. 1875-1889, Nov. 1987.

[30] C. H. Henry, "Theory of the linewidth of semiconductor lasers," *IEEE J. Quantum Electron.*, vol. QE-18, pp. 259-264, Feb. 1982.

[31] G. A. Acket, D. Lenstra, A. J. den Boef, and B. H. Verbeek, "The influence of feedback intensity on longitudinal mode properties and optical noise in index-guided semiconductor lasers," *IEEE J. Quantum Electron.*, vol. QE-20, pp. 1163-1169, Oct. 1984.

[32] K. Otsuka and H. Kawaguchi, "Period-doubling bifurcations in detuned lasers with injected signals," *Phys. Rev. A*, vol. 29, pp. 2953-2956, May 1984.

[33] J. Mink and B. H. Verbeek, "Spectral properties near threshold of index-guided AlGaAs lasers under optical feedback," in *Proc. Tenth IEEE Int. Semiconduct. Laser Conf.*, Kanazawa, Japan, Oct. 1986, pp. 200-201, paper N6.

[34] H. Ishikawa, M. Yano, and M. Takusagawa, "Mechanism of asymmetric longitudinal mode competition in InGaAsP/InP lasers," *Appl. Phys. Lett.*, vol. 40, pp. 553-555, Apr. 1982.

[35] A. Wolf, J. B. Swift, H. L. Swinney, and J. A. Vastano, "Determining Lyapunov exponents from a time series," *Physica*, vol. 16D, pp. 285-317, 1985.
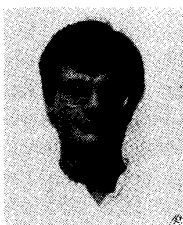
Jesper Mørk was born in Copenhagen, Denmark, on September 2, 1962. He received the M.Sc. degree in electrical engineering from the Technical University of Denmark, Lyngby, in 1986.

He is now working towards the Ph.D. degree at the Laboratory of Applied Mathematical Physics, Technical University of Denmark. His research interests include stability and nonlinear properties of semiconductor lasers with optical feedback.
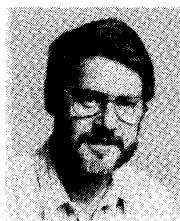
Bjarne Tromborg was born in 1940 in Denmark. He received the M.Sc. degree in physics and mathematics from the Niels Bohr Institute, Copenhagen, Denmark, in 1968.

From 1968 to 1977 he was a Research Associate at NORDITA and the Niels Bohr Institute. His research field was theoretical elementary particle physics, in particular analytic S-matrix theory and electromagnetic corrections to hadron scattering. He coauthored a research monograph on dispersion theory. From 1977 to 1979 he taught at a high school. Since 1979 he has been with the Telecommunication Research Laboratory, Copenhagen, from 1987 as Head of the Optogroup. His present research interests include stability and noise properties of semiconductor lasers, and quantum well structures in optoelectronic devices.

Mr. Tromborg received the Electroprize from the Danish Society of Engineers in 1981.
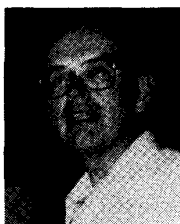
Peter L. Christiansen was born on August 6, 1937, in Vinding, Denmark. He received the M.S. degree in electrical engineering and the Ph.D. and D.Sc. degrees in applied mathematics from the Technical University of Denmark, Lyngby.

Previously, he has been a Visting Professor at the University of Michigan, Ann Arbor, the Courant Institute of Mathematical Sciences, New York University, New York, and the Italian National Research Council. Since 1981 he has been the Head of the Laboratory of Applied Mathematical Physics at the Technical University of Denmark, where he organized the Center for Modeling, Non-Linear Dynamics and Irreversible Thermodynamics (MIDIT) in 1985. He has served as Editor of *Nonlinear Science*, published by Manchester University Press, and as a referee for several international scientific journals. His research interests include asymptotic diffraction theory, and presently, nonlinear dynamics, applications to solid-state physics, optics, biophysics, and biochemistry.